JGP Journal of General Physiology

METHODS AND APPROACHES

Models to determine the kinetic mechanisms of ion-coupled transporters

Juke S. Lolkema[1] and Dirk J. Slotboom[2]

With high-resolution structures available for many ion-coupled (secondary active) transporters, a major challenge for the field is to determine how coupling is accomplished. Knowledge of the kinetic mechanism of the transport reaction, which defines the binding order of substrate and co-ions, together with the sequence with which all relevant states are visited by the transporter, will help to reveal this coupling mechanism. Here, we derived general mathematical models that can be used to analyze data from steady-state transport measurements and show how kinetic mechanisms can be derived. The models describe how the apparent maximal rate of substrate transport depends on the co-ion concentration, and vice versa, in different mechanisms. Similarly, they describe how the apparent affinity for the transported substrate is affected by the co-ion concentration and vice versa. Analyses of maximal rates and affinities permit deduction of the number of co-ions that bind before, together with, and after the substrate. Hill analysis is less informative, but in some mechanisms, it can reveal the total number of co-ions transported with the substrate. However, prior knowledge of the number of co-ions from other experimental approaches is preferred when deriving kinetic mechanisms, because the models are generally overparameterized. The models we present have wide applicability for the study of ion-coupled transporters.

Introduction

Co-ion–driven or secondary transporters constitute a major class of transporter and are found in membranes of organisms from all domains of life. In the last decade, atomic-resolution structures of many of these transporter proteins have been determined, revealing a multitude of different architectures that can be used for the transport reaction (reviewed in Forrest et al., 2011; Drew and Boudker, 2016; LeVine et al., 2016). Structures of the same transporter in different states (for instance, inward and outward facing) have revealed how various transporter architectures can support an alternate access mechanisms (for instance, Abramson et al., 2003; Yernool et al., 2004; Ressl et al., 2009; Reyes et al., 2009; Krishnamurthy and Gouaux, 2012; Perez et al., 2012; Verdon and Boudker, 2012; Kumar et al., 2014; Wöhlert et al., 2015; Malinauskaite et al., 2016; Canul-Tec et al., 2017; Garaeva et al., 2018). A major current challenge is to explain the structural basis of coupling between substrate and co-ions. This has sparked renewed interest in the kinetic mechanism of the transporters (Cleland, 1963). The abstract description of the transport reaction in a kinetic scheme describing the order of binding of substrate and co-ions and the sequence of all relevant states visited by the transporter will facilitate the understanding of the coupling mechanism at a structural level.

A co-ion–driven transporter acts on two ligands: the transported substrate and the co-ion. The rate equation gives the relation between the rate of transport and the concentrations of both ligands and is determined by the kinetic mechanism by which the transporter catalyzes the reaction. A kinetic analysis aims at determining this mechanism by fitting the rate equation to the experimental data. Thus, next to the experimental data set, rate equations for the different mechanisms must be derived. A symporter transporting a substrate together with a single co-ion catalyzes a two-substrate reaction for which the derivation of the rate equation is straightforward (Segel, 2014), but the rate equations rapidly become more complicated when the number of co-ions transported is higher than one, which is often the case. The goal of the present paper is to present a mathematical analysis yielding the rate equations for different kinetic mechanisms, valid for any number of co-ions, and allowing for mechanistic discrimination.

In the main text, a single mathematical expression is derived for the rate equation, generally applicable to the kinetic mecha-

[1]Molecular Microbiology, Groningen Biomolecular Sciences and Biotechnology Institute, University of Groningen, Groningen, The Netherlands; [2]Membrane Enzymology, Groningen Biomolecular Sciences and Biotechnology Institute, University of Groningen, Groningen, The Netherlands.

Correspondence to Dirk J. Slotboom: d.j.slotboom@rug.nl.

This work is part of the special collection entitled "Molecular Physiology of the Cell Membrane: An Integrative Perspective from Experiment and Computation."

nisms of co-ion–driven transporters. Using this expression, the dependencies of the rate on the substrate and co-ion concentrations for the different mechanisms are described. Examples, derivations, and more detailed schemes may be found in the Online supplemental material files S1–S5. In the Discussion, we focus on data analysis and show how relevant mechanistic information can be extracted from the kinetic parameters and how, in some cases, a single mechanism can be sorted out. A more detailed section on data analysis is found in the Appendix.

Results

Co-ion–driven transport

Symporters allow for the accumulation of a substrate S in a cell or organelle by coupling transport of substrate to that of one or more co-ions H. They catalyze the reaction in Eq. 1:

$$S_{out} + N\,H_{out} \rightarrow S_{in} + N\,H_{in}\,, \tag{1}$$

in which N equals the number of symported co-ions, usually protons or Na^+ ions. Free energy is transduced from the co-ion gradient to the substrate gradient. Mechanistically, secondary transporters couple the flux of the substrate to the flux of the co-ions by allowing the actual translocation step only when the transporter protein has bound the full complement of transported species at the outward-facing binding sites (the productive state; Eq. 2),

$$E + S_{out} + N\,H_{out} \rightleftarrows ESH_N \xrightarrow{k_{cat}}\,, \tag{2}$$

where k_{cat} is the catalytic rate constant. Eq. 2 describes initial rate conditions when the reverse reaction is negligible (see also the Discussion section). It follows that, for the rate of transport v (Eq. 3),

$$v = k_{cat}[ESH_N]. \tag{3}$$

The rate is determined by the population of the productive state, which in turn depends on the substrate and co-ion concentrations. A maximal rate V_{max} is obtained when all enzyme ε is in the productive state, i.e., Eq. 4,

$$V_{max} = k_{cat}\varepsilon. \tag{4}$$

The saturation level of the rate y_R in Eq. 5 follows from Eqs. 3 and 4:

$$y_R = \frac{v}{V_{max}} = \frac{[ESH_N]}{\varepsilon}\,. \tag{5}$$

Mechanisms and states

A mechanistic transporter model describes the order in which the substrate and co-ions bind to the transporter E to create productive state ESH_N via intermediate states that have a combination of free and occupied substrate and co-ion binding sites. The states may be represented by Eq. 6:

$$ES_iH_j \qquad i = 0,1 \quad j = 0,1,..N, \tag{6}$$

where a value of 0 for i and j indicates the absence of bound substrate and co-ion, respectively. The maximal values of $i = 1$ and $j = N$ indicate transport of a single substrate S coupled to transport of N co-ions. In the steady state of transport, the protein molecules are distributed over the states. The mass balance sums the concentration of all states to yield the transporter concentration ε (Eq. 7):

$$\varepsilon = \sum_{j=0}^{N}([EH_j]+[ESH_j]). \tag{7}$$

The two terms in the summation are two groups of states representing the co-ion bound to states E and ES or with $i = 0$ and $i = 1$, respectively. The distribution depends on the substrate and ligand concentrations and so does the rate of transport by Eq. 3. In the most general model, substrate and co-ions bind with no specific order (fully random), and there is no interaction between any of the binding sites. All ligands bind independently to their appropriate binding sites. More restricted mechanisms arise when substrate and co-ions bind in different combinations of random and ordered steps, leading to two types of states: An obligatory state is part of all possible pathways through the scheme, while a nonobligatory state may be bypassed. In the fully random mechanism, state E (without substrate or co-ion bound) and productive state ESH_N are the only two obligatory states. In more restricted mechanisms, intermediate states may also be obligatory, forcing the enzyme to cycle through these states.

Mechanisms are denoted here in three different ways: full schemes, simplified schemes, and textual abbreviations. Full kinetic schemes show all states, obligatory and nonobligatory, and the transitions between them. Examples are presented in Online supplemental material file S1. Simplified schemes indicate the sequence of obligatory states in the mechanism (Fig. 1). Transitions between obligatory states are termed steps and may involve random or the ordered binding of a co-ion/substrate. The textual notation of a scheme shows the substrate/co-ions that bind in each step between successive obligatory states starting at the initial state E and ending at the fully loaded transporter ESH_N. For random steps, parentheses are used to group all substrate/co-ions that can bind in any sequence (Fig. 1).

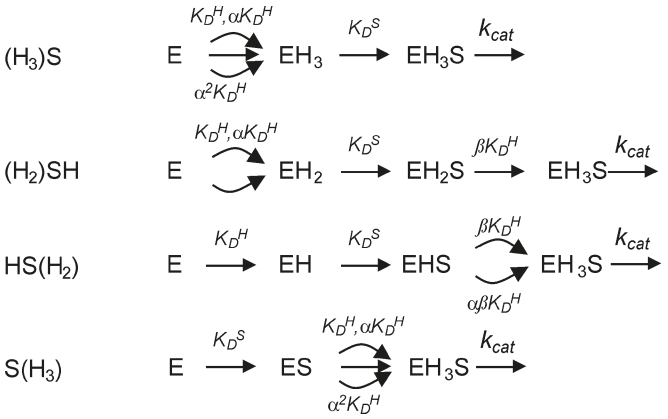

Figure 1. **Examples of textual notations (left) and simplified kinetic schemes (right) of co-ion–driven transporter mechanisms, which show a series of mechanisms where the substrate binds only after a variable number of the three co-ions have bound to the transporter.** Each transition in the simplified scheme represents a step between obligatory states. k_{cat}, catalytic rate constant; other math expressions are defined in Table 1.

Table 1. **Glossary**

Term	Definition
K_D^S	Binding constant for binding of substrate *S*
K_D^H	Binding constant for binding of co-ion *H* in successive steps
α	Interaction parameter for co-ion binding sites
β	Ratio of equilibrium constants for noninteracting co-ion binding sites
γ	Interaction parameter for co-ion and substrate binding site
x	Co-ion concentration relative to co-ion binding constant
p	Substrate concentration relative to substrate binding constant
y_R	General expression for the saturation level function of the rate
y_R^S	Saturation level function rewritten for substrate-dependent rate measurements at constant co-ion concentration
y_R^H	Saturation level function rewritten for co-ion–dependent rate measurements at constant substrate concentration

The fraction of transporter in the different states depends on the concentrations of substrate and co-ion relative to the dissociation constants K_D for co-ion binding and for substrate binding. The first possible binding event in the scheme for substrate and co-ion is characterized by the dissociation constants K_D^S and K_D^H, respectively. In later binding events, the dissociation constants are related backward to the constant of the first binding event. The relations may be simple numerical relations (ratio β) or the result of cooperativity between two binding sites (interaction parameters α between two co-ions and γ between co-ion and substrate). Several examples are presented in Online supplemental material files S1 and S2. The relations allow normalization of the concentrations of co-ion and substrate to the affinity constants K_D^S and K_D^H (normalized concentrations *x* and *p*, respectively). A glossary of the symbols is given in Table 1.

Saturation level function

The saturation level function of the rate is obtained by inserting mass balance Eq. 7 in Eq. 5, which yields Eq. 8:

$$y_R = \frac{[ESH_N]}{\sum_{j=0}^{N}([EH_j]+[ESH_j])}. \tag{8}$$

Subsequently, the concentrations of all states may be expressed in the concentrations of substrate and co-ions by using the definitions of the dissociation constants (Online supplemental material file S2.1). This results in the generalized saturation level function of the rate catalyzed by a symporter translocating the substrate with *N* co-ions,

$$y_R = \frac{[S][H]^N}{\sum_{j=0}^{N}\left(q_j K_D^S + q_{1j}[S]\right)\left(K_D^H\right)^{N-j}[H]^j} \qquad q_{1N} = 1. \tag{9}$$

In Eq. 9, each term in the summation of the denominator corresponds to one of the states. The number of terms equals the number of states in the kinetic scheme (see also Online supplemental material file S2). The power of the substrate and co-ion concentration in each term correlates with the substrate and co-ion stoichiometry of the corresponding state as in Eq. 10:

$$\text{state}ES_iH_j \leftrightarrow \text{term}\,[S]^i[H]^j \qquad i = 0,1 \; j = 0,1..N. \tag{10}$$

Maximal values for subscripts *i* and *j* correspond to the stoichiometric coefficients for substrate and co-ion in the overall transport reaction in Eq. 1, respectively. Subscripts $i = 0$ and $j = 0$ represent states with no substrate and no co-ion bound, respectively, and the corresponding substrate and co-ion concentrations are omitted from the term (in line with the power being 0). The term with the highest power in substrate and co-ion, $i = 1$ and $j = N$, corresponds to the productive state. The dissociation constants in Eq. 9 make the units of all terms identical (Eq. 11):

$$\begin{aligned}&\text{state}ES_iH_j \leftrightarrow \text{term}\left(K_D^S\right)^{1-i}[S]^i\left(K_D^H\right)^{N-j}[H]^j\\ &i = 0,1 \; j = 0,1..N.\end{aligned} \tag{11}$$

The *q* parameters (q_j and q_{1j}) contain the relational parameters α, β, and γ and determine the mechanism. The *q* parameters relate to the different states by indices *i* and *j* (Eq. 6). The q_j parameter series q_0, q_1, q_2,... corresponds to states without bound substrate, i.e., $i = 0$, whereas the complementary q_{1j} series q_{10}, q_{11}, q_{12},... corresponds to states with bound substrate, i.e., $i = 1$. The subscripts of the *q* parameters are used only to generate unique indices. Table 2 gives an overview of the different terms in the denominator of the saturation level function in Eq. 9 and the kinetic states for $N = 3$. In a fully random mechanism, all terms are present. In more restricted mechanisms, states are missing, which corresponds to *q* values of zero. Therefore, the layout of a kinetic scheme is determined by *q* values being zero or nonzero. The final term in the summation is always $[S][H]^N$ and corresponds to the productive state. Consequently, the maximal value of y_R approaches 1 at infinitely high concentrations of both the substrate and the co-ion. The *q* parameters may be obtained by deriving the saturation level function for each mechanism, which is quite laborious (Online supplemental material file S2.1). More easily, they are obtained from the full kinetic scheme. The *q* parameter for a particular state is the product of all relational parameters in the affinity constants of the transitions in a pathway traced back from the productive state to the particular state (Online supplemental material file S1.1). Table 3 presents the *q* parameters for $N = 3$.

Table 2. **Kinetic states and the saturation level function for $N = 3$**

q_j	State	$K_D^S(K_D^H)^{N-j}$	$[H]j$	q_{1j}	State	$(K_D^H)^{N-j}$	$[S][H]j$
q_0	E	$K_D^S(K_D^H)^3$	1	q_{10}	ES	$(K_D^H)^3$	$[S]$
q_1	EH	$K_D^S(K_D^H)^2$	$[H]$	q_{11}	ESH	$(K_D^H)^2$	$[S][H]$
q_2	EHH	$K_D^S K_D^H$	$[H]^2$	q_{12}	$ESHH$	K_D^H	$[S][H]^2$
q_3	$EHHH$	K_D^S	$[H]^3$	$q_{13} = 1$	$ESHHH$	1	$[S][H]^3$

The q-parameter indexing system is adequate up to $n = 9$.

Table 3. **Mechanisms and q parameters for $N = 3$**

	qij							
	q_0	q_1	q_2	q_3	q_{10}	q_{11}	q_{12}	q_{13}
State	E	EH	EHH	$EHHH$	ES	ESH	$ESHH$	$ESHHH$
(SH_3)	$\alpha^3\gamma^3$	$3\alpha^3\gamma^3$	$3\alpha^2\gamma^3$	γ^3	$\alpha^3\gamma^3$	$3\alpha^3\gamma^2$	$3\alpha^2\gamma$	1
$(SH_3)^a$	1	3	3	1	1	3	3	1
$(SH_2)H$	$\alpha\beta\gamma^2$	$2\alpha\beta\gamma^2$	$\beta\gamma^2$	0	$\alpha\beta\gamma^2$	$2\alpha\beta\gamma$	β	1
$(SH)(H_2)$	$\alpha\beta^2\gamma$	$\alpha\beta^2\gamma$	0	0	$\alpha\beta^2\gamma$	$\alpha\beta^2$	$2\alpha\beta$	1
$(SH)HH$	$\beta_1\beta_/\gamma$	$\beta_1\beta_2\gamma$	0	0	$\beta_1\beta_2\gamma$	$\beta_1\beta_2$	β_2	1
$H(SH_2)$	$\alpha\beta^2\gamma^2$	$\alpha\beta^2\gamma^2$	$2\alpha\beta\gamma^2$	γ^2	0	$\alpha\beta^2\gamma^2$	$2\alpha\beta\gamma$	1
$(H_2)(SH)$	$\alpha\beta\gamma$	$2\alpha\beta\gamma$	$\beta\gamma$	γ	0	0	$\beta\gamma$	1
$HH(SH)$	$\beta_1\beta_2\gamma$	$\beta_1\beta_2\gamma$	$\beta_2\gamma$	γ	0	0	$\beta_2\gamma$	1
$H(SH)H$	$\beta_1\beta_2\gamma$	$\beta_1\beta_2\gamma$	$\beta_2\gamma$	0	0	$\beta_1\beta_2\gamma$	β_2	1
$(H_3)S$	$\boldsymbol{\alpha^3}$	$\boldsymbol{3\alpha^3}$	$\boldsymbol{3\alpha^2}$	**1**	0	0	0	1
$(H_2)HS$	$\boldsymbol{\alpha\beta}$	$\boldsymbol{2\alpha\beta}$	$\boldsymbol{\beta}$	**1**	0	0	0	1
$H(H_2)S$	$\boldsymbol{\alpha\beta^2}$	$\boldsymbol{\alpha\beta^2}$	$\boldsymbol{2\alpha\beta}$	**1**	0	0	0	1
$HHHS$	$\boldsymbol{\beta_1\beta_2}$	$\boldsymbol{\beta_1\beta_2}$	$\boldsymbol{\beta_2}$	**1**	0	0	0	1
$(H_2)SH$	$\alpha\beta$	$2\alpha\beta$	β	0	0	0	β	1
$HHSH$	$\beta_1\beta_2$	$\beta_1\beta_2$	β_2	0	0	0	β_2	1
$HS(H_2)$	$\alpha\beta^2$	$\alpha\beta^2$	0	0	0	$\alpha\beta^2$	$2\alpha\beta$	1
$HSHH$	$\beta_1\beta_2$	$\beta_1\beta_2$	0	0	0	$\beta_1\beta_2$	β_2	1
$S(H_3)$	α^3	0	0	0	$\boldsymbol{\alpha^3}$	$\boldsymbol{3\,\alpha^3}$	$\boldsymbol{3\,\alpha^2}$	**1**
$S(H_2)H$	$\alpha\beta$	0	0	0	$\boldsymbol{\alpha\beta}$	$\boldsymbol{2\alpha\beta}$	$\boldsymbol{\beta}$	**1**
$SH(H_2)$	$\alpha\beta^2$	0	0	0	$\boldsymbol{\alpha\beta^2}$	$\boldsymbol{\alpha\beta^2}$	$\boldsymbol{2\alpha\beta}$	**1**
$SHHH$	$\beta_1\beta_2$	0	0	0	$\boldsymbol{\beta_1\beta_2}$	$\boldsymbol{\beta_1\beta_2}$	$\boldsymbol{\beta_2}$	**1**

The top part shows mechanisms with random binding of the substrate and (part of) the co-ions, and the bottom part shows mechanisms with ordered binding of the substrate. Bold entries show the q parameters for co-ion binding in the response model (Online supplementary material file S3).
[a]Fully random with no interaction between the sites: $\alpha = 1$, $\gamma = 1$.

Substrate-dependent measurements at fixed co-ion concentration

Rate equation

Rewriting the general saturation level function in Eq. 9 for substrate-dependent measurements by separating the terms containing the substrate concentration and the co-ion concentration yields Eq. 12:

$$y_R^S = \frac{[H]^N}{\sum_{j=0}^{N} q_{1j}(K_D^H)^{N-j}[H]^j} \frac{[S]}{K_D^S \frac{\sum_{j=0}^{N} q_j (K_D^H)^{N-j}[H]^j}{\sum_{j=0}^{N} q_{1j}(K_D^H)^{N-j}[H]^j} + [S]}. \quad (12)$$

Superscript S refers to substrate-dependent measurements at constant co-ion concentration. It follows that the general expression for the rate equation in substrate-dependent rate measurements is a simple hyperbolic function (Eqs. 13 and 14),

$$y_R^S = y_R^{max} \frac{[S]}{K_D^S(app) + [S]}, \quad (13)$$

with

$$y_R^{max} = \frac{[H]^N}{\sum_{j=0}^{N} q_{1j} (K_D^H)^{N-j} [H]^j}$$
$$K_D^S(app) = K_D^S \frac{\sum_{j=0}^{N} q_j (K_D^H)^{N-j} [H]^j}{\sum_{j=0}^{N} q_{1j} (K_D^H)^{N-j} [H]^j}, \quad (14)$$

with both the maximal rate and the apparent affinity for the substrate depending on the co-ion.

Maximal rate

The maximal saturation level y_R^{max} (Eq. 14) depends on the states that are substrate bound (q_{1j} parameters). With $N = 3$, there are eight mechanisms, in which all q_{1j} parameters are nonzero, and therefore, all possible substrate-bound states are present (the mechanisms (SH_3), $(SH_2)H$, $(SH)(H_2)$, $(SH)H$, $S(H_3)$, $S(H_2)H$, $SH(H_2)$, and SHHH; Table 3). For these mechanisms, the highest power of the co-ion concentration in the denominator of y_R^{max} equals N (Eq. 14). In four mechanisms, $H(SH_2)$, $H(SH)H$, $HS(H_2)$, and HSHH, state *ES* is absent from the scheme ($q_{10} = 0$), yielding (Eq. 15):

$$y_R^{max} = \frac{[H]^{N-1}}{q_{11}(K_D^H)^{N-1} + q_{12}(K_D^H)^{N-2}[H] + \ldots + [H]^{N-1}} \qquad q_{10} = 0, \quad (15)$$

and the highest power of the co-ion concentration is $(N - 1)$. In mechanisms $(H_2)(SH)$, $HH(SH)$, $(H_2)SH$, and HHSH, states *ES* and *ESH* are both absent ($q_{10} = q_{11} = 0$), yielding an equation with the highest power $N - 2$ in the denominator (Eq. 16),

$$y_R^{max} = \frac{[H]^{N-2}}{q_{12}(K_D^H)^{N-2} + \ldots + [H]^{N-2}} \qquad q_{10} = q_{11} = 0, \quad (16)$$

and in mechanisms $(H_3)S$, $(H_2)HS$, $H(H_2)S$, and HHHS, none of the substrate-bound states exist, except for the productive state ESH_N, and the maximal saturation level reduces to (Eq. 17)

$$y_R^{max} = \frac{[H]^N}{[H]^N} = 1 \qquad q_{10} \ldots q_{1N-1} = 0. \quad (17)$$

The analysis shows that the highest power of the co-ion concentration in the maximal rate equation indicates the number of co-ions that bind in a random step together with the substrate plus the number of co-ions that bind in the steps thereafter. It can be shown that the expression for y_R^{max} is identical to the saturation level function of binding of this subset of co-ions (Online supplemental material file S3). This information can be used to discriminate between mechanisms (Fig. 2). Maximal rates from substrate-dependent rate measurements that are independent of the co-ion concentration indicate that the final step is the ordered binding of the substrate to the obligatory EH_N state, with all co-ions already bound. For instance, in the $(H_3)S$ mechanism, productive state ESH_N is the only state with substrate bound. Maximal rates that are dependent on the co-ion concentration indicate co-ion binding in the final step.

Affinity for the substrate

The general expression for the ratio of the apparent affinity and the affinity in the first substrate-binding step (Eq. 14) may be written as Eq. 18:

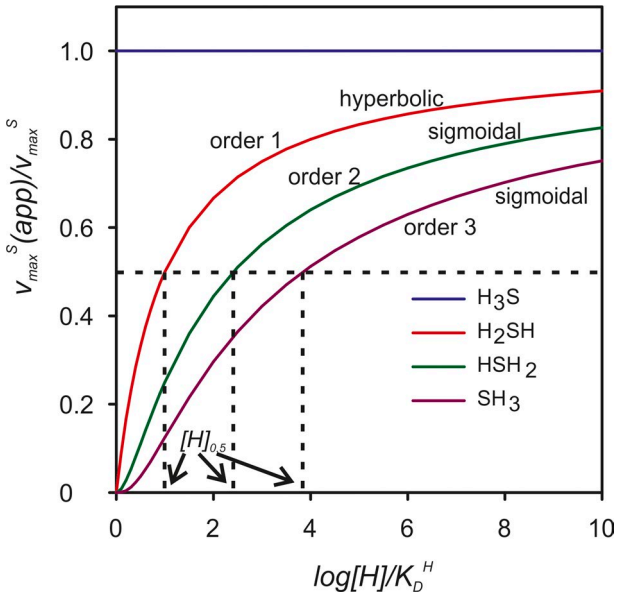

Figure 2. **Apparent maximal rate in substrate-dependent rate measurements.** Simulation of Eq. 14 for mechanisms $(H_3)S$, $(H_2)SH$, $HS(H_2)$, and $S(H_3)$. All interaction parameters were set to 1. Arrows indicate the co-ion concentration $[H]_{0.5}$, at which the measured maximal rate is half the true maximal rate (maximal saturation level = 0.5). Terms are defined in Tables 1 and 5.

$$\frac{K_D^S(app)}{K_D^S} = \frac{q_0 + q_1 x + \ldots q_{N-1} x^{N-1} + q_N x^N}{q_{10} + q_{11} x + \ldots q_{1N-1} x^{N-1} + q_{1N} x^N}, \quad (18)$$

in which x is the relative co-ion concentration ($x = [H]/K_D^H$) at which the measurement is done. Apparent affinity measurements for the substrate at different fixed co-ion concentrations can help to discriminate between different mechanisms because the dependence on the co-ion concentration in the extreme low- and high-concentration domains of the co-ion ($x << 1$ and $x >> 1$, respectively) is different for the various kinetic schemes. The terms of the summation in the denominator of Eq. 18 correspond to the substrate-bound states (q_{1j}), and those in the numerator correspond to states without bound substrate (q_j). As is illustrated below, in double logarithmic plots of the relative apparent affinity for the substrate ($K_D^S(app)/K_D^S$) versus the relative co-ion concentration (x), linear regions may be observed at the low– and high–co-ion concentration extremes (Fig. 3; Zhang et al., 2007). The slope of the linear regions in the low-concentration domain reports the number of co-ions binding in the steps before the substrate-binding step. The slope of the line in the high-concentration domain reports the number of co-ions binding in the steps following the substrate-binding steps. Co-ions that bind randomly with the substrate in the substrate-binding step do not contribute to the apparent affinity. The rule is independent of N. Note the different information in the affinity for the substrate in the high-concentration domain and the maximal saturation level in substrate-dependent measurements (see the Maximal rate section). The former reports the number of co-ions in the steps after the binding of the substrate, and the latter reports the number of co-ions that bind in the substrate-binding step plus those binding in the steps thereafter.

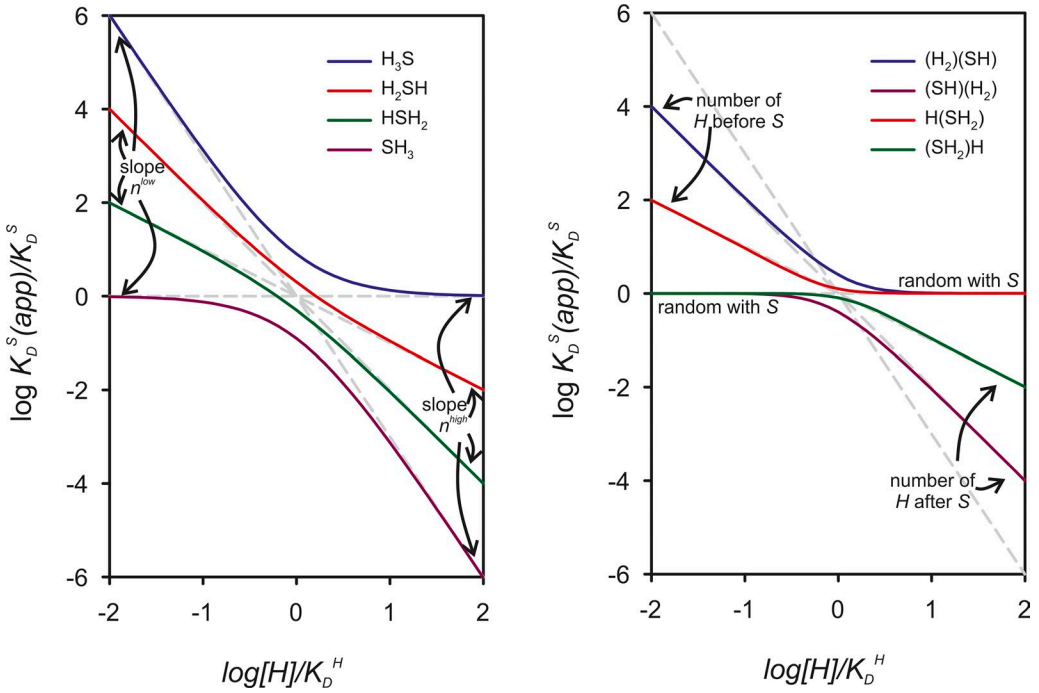

Figure 3. **Apparent affinity for the substrate in substrate-dependent rate measurements.** Simulations of Eq. 18 for mechanisms with ordered (left) and random (right) binding of the substrate and co-ions. All interaction parameters were set to 1. The dashed lines interpolate the linear regions in the low– and high–co-ion concentration domains. Arrows indicate regions where constants detailed in Table 5 may be extracted from the data. Other terms are defined in Table 1.

We illustrate the behavior in the low– and high–co-ion concentration domain by analyzing the q parameters in Table 3 being zero or nonzero in the different mechanisms. In fully random mechanisms (SH_3), all q parameters are nonzero (Table 3), and it follows from Eq. 18 at very low and very high co-ion concentrations that

$$(SH_3) \qquad \begin{aligned} \frac{K_D^S(app)}{K_D^S} &= \frac{q_0}{q_{10}} = 1 \quad x \ll 1 \\ \frac{K_D^S(app)}{K_D^S} &= q_N = \gamma^3 \quad x \gg 1. \end{aligned} \tag{19}$$

In both domains, the apparent affinity is independent of the co-ion concentration, indicating that none of the co-ions binds in an obligatory step before or after the substrate. Potential interaction between substrate and co-ion binding sites (captured in parameter γ) is evident in the high-concentration domain.

The other mechanisms fall into three groups: those that miss substrate-bound states and affect the denominator in Eq. 18, those that miss states with no substrate bound and affect the numerator, and those that miss both of these types of states. We will illustrate the information that can be extracted from apparent affinity measurements using the example of kinetic schemes with $N = 3$.

The group that misses substrate-bound states contains the mechanisms $H(SH_2)$, $(H_2)(SH)$, $HH(SH)$, $(H_3)S$, $(H_2)HS$, $H(H_2)S$, and HHHS. The $H(SH_2)$ mechanism misses state ES and $q_{10} = 0$. Then, Eq. 18 is

$$\frac{K_D^S(app)}{K_D^S} = \frac{1}{x}\frac{q_0 + q_1 x + \ldots q_{N-1}x^{N-1} + q_N x^N}{q_{11} + \ldots q_{1N-1}x^{N-2} + x^{N-1}}, \tag{20}$$

and the extremes are

$$q_{10} = 0 \qquad \begin{aligned} \frac{K_D^S(app)}{K_D^S} &= \frac{q_0}{q_{11}x} \quad x \ll 1 \\ \frac{K_D^S(app)}{K_D^S} &= q_N \quad x \gg 1. \end{aligned} \tag{21}$$

It follows that, while in the high-concentration domain the ratio does not depend on the co-ion, it does in the low-concentration domain. In a double logarithmic plot of the affinity versus the co-ion concentration, the slope is –1 at $x << 1$ and 0 at $x >> 1$. In the $(H_2)(SH)$ and $HH(SH)$ mechanisms, both states ES and ESH are missing, and the extremes are

$$q_{10} = q_{11} = 0 \qquad \begin{aligned} \frac{K_D^S(app)}{K_D^S} &= \frac{q_0}{q_{12}x^2} \quad x \ll 1 \\ \frac{K_D^S(app)}{K_D^S} &= q_N \quad x \gg 1. \end{aligned} \tag{22}$$

The slope of the line in the double reciprocal plot is –2 in the low-concentration domain, while still 0 in the high-concentration domain. In the $(H_3)S$, $(H_2)HS$, $H(H_2)S$, and HHHS mechanisms q_{10} up to q_{1N-1} all are 0, and the slope in the low-affinity domain equals $-N$, while in the high-affinity domain, the ratio does not depend on the co-ion concentration.

In the second group, state EH_N is missing in the $(SH_2)H$ mechanism. With $q_N = 0$, Eq. 18 results in

$$\frac{K_D^S(app)}{K_D^S} = \frac{q_0 + q_1 x + \ldots q_{N-1}x^{N-1}}{q_{10} + q_{11}x + \ldots q_{1N-1}x^{N-1} + q_{1N}x^N}, \tag{23}$$

and it follows for the extremes that

$$q_N = 0 \qquad \begin{aligned} \frac{K_D^S(app)}{K_D^S} &= \frac{q_0}{q_{10}} = 1 \quad x \ll 1 \\ \frac{K_D^S(app)}{K_D^S} &= \frac{q_{N-1}}{x} \quad x \gg 1. \end{aligned} \tag{24}$$

Hence, the slope of the line in the double logarithmic plot does not depend on the co-ion in the low-concentration domain but does in the high-concentration domain where the slope is −1. Similarly, in the (SH)(H_2) and (SH)HH mechanisms lacking both states EH_N and EH_{N-1}, it follows that

$$q_N = q_{N-1} = 0 \quad \frac{K_D^S(app)}{K_D^S} = \frac{q_0}{q_{10}} = 1 \quad x \ll 1 \qquad \frac{K_D^S(app)}{K_D^S} = \frac{q_{N-2}}{x^2} \quad x \gg 1, \tag{25}$$

and, in the double logarithmic plot, the slopes of the lines in the low- and high-concentration domains are 0 and −2, respectively. With q_N down to q_1 all being zero in mechanisms S(H_3), S(H_2)H, SH(H_2), and SHHH, the slopes are 0 and −N, respectively. The slope in the high-concentration domain reports in this category of mechanisms the number of co-ions that bind in steps after the step in which the substrate binds.

Finally, in the last group, states EH_N and ES are missing in the H(SH)H mechanism, and $q_N = q_{10} = 0$. Then, Eq. 18 is

$$\frac{K_D^S(app)}{K_D^S} = \frac{1}{x}\frac{q_0 + q_1 x + \ldots q_{N-1}x^{N-1}}{q_{11} + \ldots q_{1N-1}x^{N-2} + x^{N-1}}, \tag{26}$$

and the extremes are

$$q_N = q_{10} = 0 \quad \frac{K_D^S(app)}{K_D^S} = \frac{q_0}{q_{11}x} \quad x \ll 1 \qquad \frac{K_D^S(app)}{K_D^S} = \frac{q_{N-1}}{x} \quad x \gg 1. \tag{27}$$

The slopes in the low- and high-concentration domains of the double logarithmic plot are both −1. Similarly, it can be shown that in the (H_2)SH and HHSH mechanisms where $q_N = q_{10} = q_{11} = 0$, the slope in the low-concentration domain is −2 and in the high-concentration domain −1, and in the HS(H_2) and HSHH mechanisms, the slopes are −1 and −2, respectively. Consistent with the other two categories, the slopes in the low- and high-concentration domains report the number of co-ions in the steps before and after the substrate-binding step. It is noteworthy that Eq. 18 may be generalized for mechanisms with ordered binding of the substrate (Table 3, bottom part), by expressing $K_D{}^S(app)$ in the saturation level function of binding of the co-ions that bind before and after the substrate, as is detailed in Online supplemental material file S3.

Co-ion–dependent measurements at fixed substrate concentration

Rate equation and maximal rates

Rewriting the general saturation level function in Eq. 9 for co-ion–dependent measurements by separating the terms containing the substrate concentration and the co-ion concentration yields

$$y_{R\,H} = \frac{[S]}{q_N K_D^S + [S]} \frac{[H]^N}{\frac{\sum_{j=0}^{N-1}\left(q_j K_D^S + q_{1j}[S]\right)(K_D^H)^{N-j}[H]^j}{q_N K_D^S + [S]} + [H]^N}. \tag{28}$$

Superscript H refers to co-ion–dependent measurements at constant substrate concentration.

Eq. 28 is of the form

$$y_R^H = y_R^{max}\frac{[H]^N}{\sum\ldots\ldots\ldots + [H]^N} \tag{29}$$

with

$$y_R^{max} = \frac{[S]}{q_N K_D^S + [S]}. \tag{30}$$

The maximal rate increases hyperbolically with the substrate concentration. A special case is obtained for q_N is zero when the maximal rate is independent of the substrate concentration ($y_R{}^{max} = 1$), which corresponds to the absence of state EH_N (Table 3). The formation of productive state EH_NS must originate from state $EH_{N-1}S$ by binding of a co-ion. The maximal rate from co-ion–dependent rate measurement is independent of the substrate concentration when the final step in the mechanism is the binding of a co-ion to the obligatory state $EH_{N-1}S$. Maximal rates that depend on the substrate concentration indicate that substrate binding is part of the final step in the mechanism.

Experimentally, the apparent affinity for the co-ion K_A is the co-ion concentration that results in half of the maximal rate. Combining Eqs. 28 and 30 yields the following expression:

$$\frac{y_R^H}{y_R^{max}} = \frac{1}{2} = \frac{K_A{}^N}{\frac{\sum_{j=0}^{N-1}\left(q_j K_D^S + q_{1j}[S]\right)(K_D^H)^{N-j}K_A{}^j}{q_N K_D^S + [S]} + K_A{}^N}. \tag{31}$$

It follows that

$$\left(\frac{K_A}{K_D^H}\right)^N = \frac{\sum_{j=0}^{N-1}\left(q_j K_D^S + q_{1j}[S]\right)\left(\frac{K_A}{K_D^H}\right)^j}{q_N K_D^S + [S]}, \tag{32}$$

showing that there is not a simple relation between the half-saturation concentration and the affinity constants in the kinetic scheme.

Mechanistic Hill analysis

At constant substrate concentration, the rate saturates relative to $y_R{}^{max}$,

$$y = \frac{y_R^H}{y_R^{max}}, \tag{33}$$

which is a sigmoidal function of order N, the number of co-ions involved in the transport reaction. By substituting Eq. 28, it follows for the Hill analysis equation (Hill, 1910; Online supplementary material file S4) that

$$\frac{y}{1-y} = \frac{[H]^N}{\sum_{j=0}^{N-1}\frac{q_j K_D^S + q_{1j}[S]}{q_N K_D^S + [S]}(K_D^H)^{N-j}[H]^j}. \tag{34}$$

Separating out the first and the last terms in the sum of the denominator while switching to relative concentrations, $x = [H]/K_D{}^H$ for the co-ion yields

$$\frac{y}{1-y} = \frac{x^N}{\frac{q_0 K_D^S + q_{10}[S]}{q_N K_D^S + [S]} + \sum_{j=1}^{N-2}\frac{q_j K_D^S + q_{1j}[S]}{q_N K_D^S + [S]}x^j + \frac{q_{N-1}K_D^S + q_{1N-1}[S]}{q_N K_D^S + [S]}x^{N-1}}. \tag{35}$$

The first term in the sum in the denominator corresponds to the states E and ES (q_0 and q_{10}) and is independent of the co-ion concentration ($j = 0$). The remaining terms do depend on the co-ion concentration and correspond to states with partially occupied co-ion binding sites (j =1 to $N - 1$). Ignoring the partially occupied states transforms Eq. 35 into the form of the original Hill analysis function demonstrating the assumptions made in the Hill approach

$$\frac{y}{1-y} = \frac{[H]^n}{K_A{}^n}. \tag{36}$$

While the Hill analysis–based function in Eq. 36 results in a linear relation with Hill coefficient n as the slope in a double logarithmic plot of $y/(1 - y)$ versus $[H]$, the same analysis based on a mechanistic description of the transport reaction (Eq. 35) does not result in such a linear relation, and the slope obtained is a variable depending on the co-ion concentration (Wyman and Gill, 1990). In contrast to Hill coefficient n in Eq. 36, N in Eq. 35 corresponds to the number of co-ion binding sites.

In the low-concentration domain of the co-ion, only the first term survives in the denominator of Eq. 35, yielding

$$\frac{y}{1-y} = \frac{q_N K_D^S + [S]}{q_0 K_D^S + q_{10}[S]} x^N \qquad x \ll 1. \tag{37}$$

The double logarithmic plot is a straight line in this limit with a slope of N. In the other extreme, high co-ion concentrations, the last term remains, and

$$\frac{y}{1-y} = \frac{q_N K_D^S + [S]}{q_{N-1} K_D^S + q_{1N-1}[S]} x \qquad x \gg 1. \tag{38}$$

The double logarithmic plot reveals a linear part with a slope of 1 in the high concentration limit. The slope decreases from a value corresponding to the number of binding sites N at low co-ion concentration down to a value of 1 at high co-ion concentration (Weiss, 1997; Yifrach, 2004; Fig. 4). The Hill coefficient n (lowercase n, not N, the number of co-ions) for mechanistic models is defined at the co-ion concentration equal to the affinity constant K_A or the first derivative of the double logarithmic plot at log $y/1 - y = 0$, i.e., at the x-axis intercept (Kuriyan et al., 2013).

The constant substrate concentration affects the Hill coefficient n in different ways, depending on the mechanism. In a fully random mechanism (SH_N) with no interaction between the substrate and co-ion binding sites ($q_j = q_{1j}$ and $q_N = 1$), Eq. 34 reduces to

$$\frac{y}{1-y} = \frac{x^N}{q_j \sum_{j=0}^{N-1} x^j} \qquad q_j = q_{1j} \quad q_N = 1, \tag{39}$$

and the Hill coefficient, like the apparent affinity constant K_A, is independent of the substrate concentration. In the $(H_3)S$, $(H_2)HS$, $H(H_2)S$, and HHHS mechanisms where $q_0..q_{N-1} = 0$ and $q_N = 1$ (Table 3), it follows that

$$\frac{y}{1-y} = \frac{x^N}{\frac{K_D^S}{K_D^S + [S]} \sum_{j=0}^{N-1} q_j x^j} \qquad q_{10}...q_{N-1} = 0 \quad q_N = 1. \tag{40}$$

The term before the summation that contains the substrate concentration does not affect the shape of the first derivative

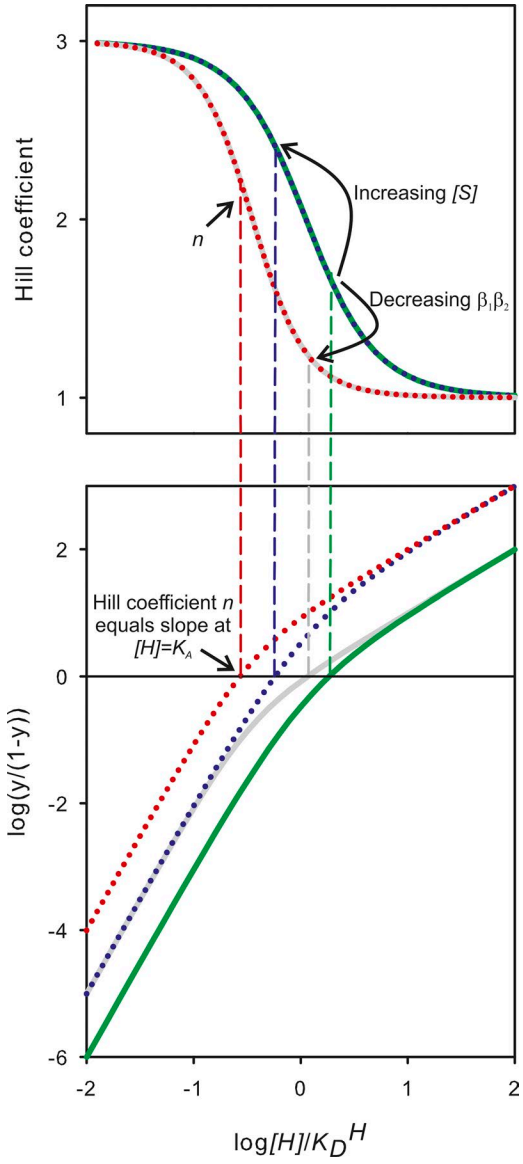

Figure 4. **Mechanistic Hill analysis of transporter mechanism HHHS (n = 3).** Simulation of the double logarithmic plot of the Hill equation (bottom) and the first derivative (top). The Hill equation of the HHHS mechanism is $[y/(1 - y)] = \{x^3/\{(\beta_2 K_D^\delta/(K_D^\delta + [S]))(\beta_1 + \beta_1 x + x^2)\}$. The affinity constant $K_A/K_D{}^H$ is the value of $[H]/K_D{}^H$ at the x-axis intercept in the bottom plot, and the mechanistic Hill coefficient n is the value of the first derivative in the top plot at $K_A/K_D{}^H$; β is the ratio of equilibrium constants for noninteracting co-ion binding sites, $K_D{}^H$ is the binding constant for binding of co-ion H in successive steps, and $K_D{}^S$ is the binding constant for binding of substrate S. Blue and green curves demonstrate the effect of changing the substrate concentration. Increasing the substrate concentration shifts the curves up by an amount of $\log(K_D{}^S + [S])$, and consequently, the intercept with the ordinate K_A goes down and the Hill coefficient n goes up. The same holds for the difference between the gray and red curves. Comparison of blue and red curves (and similarly of green and gray curves) shows the effect of changing the q parameters (Table 4).

in the double-reciprocal plot, but variation in the substrate concentration does affect the K_A value, and consequently, the Hill coefficient n varies by moving up and down the same first-derivative curve. Increasing $[S]$ will result in higher values of the Hill coefficient n, until the maximal value N is reached (Fig. 4). For mechanisms $(H_3)S$, $(H_2)HS$, $H(H_2)S$, and

Table 4. **Parameters affecting the values of the Hill coefficient and K_A**

$KDS/(KDS + [S])$	β_1	β_2	n	KA	Curve
1	1	1	1.6	1.91	Blue
0.1	1	1	2.3	0.59	Green
1	0.1	1	1.2	1.22	Red dashed
0.1	0.1	1	2.1	0.28	Gray dashed

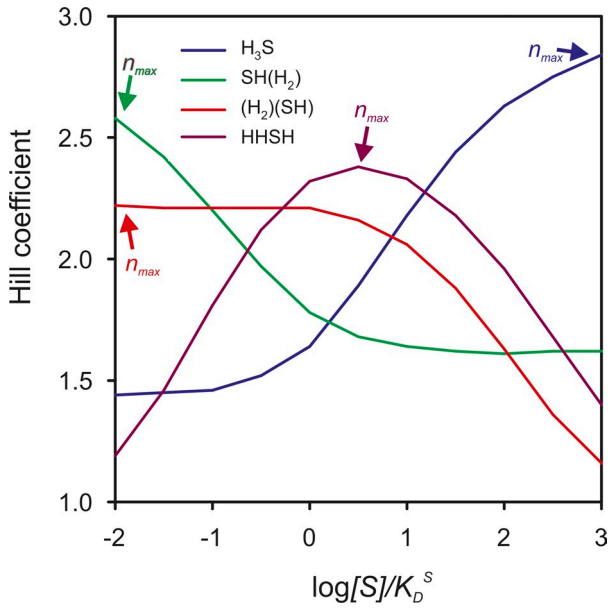

Figure 5. **The relation between the Hill coefficient and the substrate concentration in the $(H_3)S$, $SH(H_2)$, $(H_2)(SH)$, and HHSH mechanisms.** Terms are defined in Tables 1 and 5.

HHHS, mechanisms in which the substrate exclusively binds in the final step, the mechanistic Hill analysis provides a way to determine the number of binding sites N (Lolkema and Slotboom, 2015).

For all other mechanisms, the substrate concentration is in (part of) the terms in the sum of Eq. 34, and the relation between the substrate concentration and the Hill coefficient is more complicated and has many faces (Fig. 5). In none of these mechanisms does the Hill coefficient extrapolate to the number of binding sites N at high substrate concentration. The information on the number of binding sites is lost, and the discrimination between different mechanisms is poor.

Discussion

Experimental conditions for model use

In the analysis described here, the transporter is treated as an enzyme (E) that compulsorily requires more than one substrate: the species targeted to be transported (S) and one or more (identical) co-ions (H). The kinetic models describe equilibrium binding of the full complement of substrate and co-ions to the state with the outward-facing binding sites (ESH_N), after which isomerization to the inward-facing state takes place, followed by dissociation into the cytoplasm (in vivo) or vesicle lumen (in vitro) and reorientation of the "empty" binding sites into the outward-facing state. Consequently, the catalytic rate constant k_{cat} includes the rate constants for the isomerization of the binding sites in both the loaded and unloaded states and the dissociation constants of the substrate and co-ions at the cytoplasmic face of the membrane. The derived rate equations describe the steady-state rate of uptake from the external medium to the cytoplasm or the lumen under initial rate conditions; that is, binding of cytoplasmic or luminal substrate or co-ion is negligible, because either the concentration is zero or it is far below the dissociation constant of the inward-facing binding site. The latter may be difficult to control in vivo, or when the co-ion is proton, but quite feasible in vitro in case of Na^+-driven transporters. It is noteworthy that the goal of this paper was not to discuss the different transport modes or assay techniques (i.e., exchange, counterflow, pre–steady state, and single molecule).

q parameters: Model dependence

According to general Eq. 9, the rate of transport catalyzed by a symporter is proportional to the fraction of the enzyme in productive state ESH_N as expressed in Eq. 8. The denominator corresponds to the mass balance—i.e., the summation of the concentrations of all kinetic states. Each term in the summation corresponds to one state. The different mechanisms are defined by the q parameters in the general equation, as presented in the q table (Table 3). The q parameters are read directly from the transitions in the kinetic scheme. The number of q parameters equals $2(N + 1)$, one for each state with a particular number of ligands, substrate or co-ions, bound. In the common case where only a single substrate molecule is transported, this results in two sets of q parameters, q_j and q_{1j}, representing substrate-free and substrate-bound states, respectively, with $j = 0$ to N numbers of co-ion bound. The q table in Table 3 represents a mechanism in which the initial binding to the different co-ion binding sites is identical (symmetrical binding) as if the binding was to the identical subunits of a multimer. In more realistic transporter mechanisms, different states with the same number of co-ions bound exist, for instance, EH_A and EH_B, in which the binding site for co-ion H_A is not identical to that of H_B. In such cases, the q parameters contain contributions from both states (Online supplemental material file S3, section 5). The equilibrium shift–ordered mechanism discussed in Online supplemental material file S5, section 3, provides another example with more complex q parameters.

Data analysis

A detailed strategy for data analysis is presented in the Appendix. Here we will give a summary of the main steps. Combi-

Table 5. **Constants derived from kinetic parameters**

Constant[a]	Source	Definition
$[S]_{0.5}$	$V_{max}{}^{H}(app)$	Half saturation of the maximal rate in co-ion–dependent rate measurements (Eq. 31)
$[H]_{0.5}$	$V_{max}{}^{S}(app)$	Half saturation of the maximal rate in substrate-dependent rate measurements (Fig. 2)
$K_D{}^{S}(app)^{high}$	$K_D{}^{S}(app)$	Limit of apparent affinity in the high–co-ion concentration domain (Fig. 3)
$K_D{}^{S}(app)^{low}$	$K_D{}^{S}(app)$	Limit of apparent affinity in the low–co-ion concentration domain (Fig. 3)
$[H]_{y=0}$	$K_D{}^{S}(app)$	Intercept of linear parts of apparent affinities in the low– and high–co-ion concentration domains (Online supplemental material, Figure S4.2)
n^{high}	$K_D{}^{S}(app)$	Number of co-ions from slope linear part in the high–co-ion concentration domain (Fig. 3)
n^{low}	$K_D{}^{S}(app)$	Number of co-ions from slope linear part in the low–co-ion concentration domain (Fig. 3)
$n_{N\text{-}t}$	$V_{max}{}^{S}(app)$	Hill coefficient of maximal rate in substrate-dependent rate measurements
n_{max}	$n(app)$	Highest Hill coefficient of co-ion–dependent rate measurements (Fig. 5)

[a]t is the number of co-ions binding before the substrate (Online supplementary material file S3).

nations of random and ordered binding steps of substrate and co-ions to the transporter make the different mechanisms. In a fully random mechanism, all possible states are present and represented by a q parameter. Ordered binding results in the absence of states in the scheme, and the corresponding q parameters are zero, which results in specific characteristics of the rate equation that may allow for tracing back the mechanism from the experimental data. The analysis requires rate measurements where the concentration of one ligand is varied while the other is kept constant—i.e., substrate-dependent rate measurements at constant co-ion concentration and co-ion–dependent rate measurements at constant substrate concentration. The information is largely contained in the dependence of the extracted parameters on the constant second substrate. The parameters are maximal rates, affinity constants, and Hill coefficients. The parameters may be independent of the second substrate, or the relation may be hyperbolic or sigmoidal. The same mechanistic characteristic may be presented by more than one parameter. This is an advantage since experimental limitations may not allow one to obtain all necessary relations or at the required precision. For instance, if a parameter appears independent of the second substrate, it is possible that the concentration range tested for the second substrate was too narrow, and conclusive interpretation may not be possible. However, if a dependency is observed, firm mechanistic interpretation of the data is possible.

With an increasing number of co-ions transported, the number of possible mechanisms increases rapidly, and in these cases the full elucidation of the kinetic mechanism may not be possible, because parameters become unidentifiable (Middendorf and Aldrich, 2017a,b). Nonetheless, useful information can still be extracted by narrowing down the possibilities to a subset of mechanisms. Although in principle the number of co-ions used in the transport reaction can be determined in the analysis, in practice it is helpful to know this number beforehand—for instance, from reversal potential measurements, or from uptake experiments, using radiolabeled substrate and co-ion (Accardi and Miller, 2004; Groeneveld and Slotboom, 2010; Fitzgerald et al., 2017).

Analysis of maximal rates of transport

Several examples of data analysis are given in the Appendix. Maximal rates $V_{max}{}^{S}(app)$ and $V_{max}{}^{H}(app)$ from substrate- and co-ion–dependent rate measurements (Table 5; and Appendix, Table A1), respectively, are the most informative parameters and, in addition, usually determined with the highest accuracy. The analyses given in the "Maximal rate" and "Rate equations and maximal rates" sections show that the dependence of the maximal rates on the second substrate identify ordered binding of substrate or co-ion in the (obligatory) final step. There are three possible combinations: (1) $V_{max}{}^{S}(app)$ is dependent and $V_{max}{}^{H}(app)$ is independent; (2) $V_{max}{}^{S}(app)$ is independent and $V_{max}{}^{H}(app)$ is dependent; and (3) both are dependent. In combination 1, the final step involves the binding of only co-ions; in combination 2, the final step involves ordered binding of the substrate; and in combination 3, random binding of both substrate and co-ion binding are involved in the final step.

Both maximal rate $V_{max}{}^{S}(app)$ and the affinity for the substrate in substrate-dependent rate measurements $K_D{}^{S}(app)$ discriminate between different mechanisms by reporting the number of co-ions that bind before, together with, or after the substrate. The number of co-ions that bind in the substrate-binding step plus those in the steps thereafter corresponds to the highest power of the co-ion concentration in $V_{max}{}^{S}(app)$ ("Maximal rate" section). While this relationship may be easy to assess for powers of 0 or 1 when the relation is independent (combination 2 above) or hyperbolic, for higher powers, leading to sigmoidal relations, accurate determination of the power is usually not possible (Fig. 2). A Hill-type analysis of the experimental data relating the maximal rate to the co-ion concentration yields a Hill coefficient that reflects the minimal value of the highest power and, consequently, the minimum number of co-ions that bind in the substrate-binding step and in the steps thereafter (see below under heading "The Hill coefficient").

Analysis of substrate affinities

Besides the maximal rates, the substrate affinity also provides useful information on the mechanism. A double logarithmic plot of $K_D{}^{S}(app)$ and the co-ion concentration reveals linear parts in

the low– and high–co-ion concentration domains (Zhang et al., 2007). The slopes correspond to the number of co-ions binding before and after the substrate. Co-ions that bind randomly with the substrate do not contribute. Consequently, the sum of the slopes from the higher and lower domains adds up to the number of co-ions *N* only when substrate binding is ordered (see also Online supplemental material file S3).

The Hill coefficient

The mechanistic analysis of co-ion–dependent rate measurements shows that in addition to maximal rate $V_{max}{}^{H}(app)$ discussed above, both the affinity constant and Hill coefficient deduced from the data depend on the constant substrate concentration (Co-ion–dependent measurements at fixed substrate concentration section). The shape of the general saturation level function in Eq. 28 is dependent on the number of co-ions *N*, but a fit of the data will in only rare cases yield a reliable result, as the system is overparameterized. The Hill coefficient is not an explicit parameter in Eq. 28 but is a measure of the shape. Albeit formally incorrect, the Hill coefficient may be determined by fitting the data to Hill Eq. 36. Numerical analyses demonstrate that the error introduced by fitting the data to the wrong equation is acceptable considering experimental error in the data set (Online supplemental material file S5.6). By definition, Hill coefficient *n* is the slope of the curve in a double logarithmic plot of the Hill function $y/(1 - y)$ and the co-ion concentration where the saturation level is $y = 0.5$ (Fig. 4). In the mechanistic description, the Hill coefficient is a variable depending on the co-ion concentration (Wyman and Gill, 1990). As discussed many times before for binding phenomena involving more than one ligand, also here, the Hill coefficient does not correlate with the number of co-ions in the transport reaction but is a number between 1 and *N* depending on the other parameters in the system (Wyman and Gill, 1990; Lolkema and Slotboom, 2015). The Hill coefficient reports the minimal value for *N*. Substrate concentration $[S]$ provides an experimental handle to manipulate the value of *n*, but the effect of $[S]$ on the value of *n* strongly depends on the mechanism. In those mechanisms where the substrate binds ordered in the final step thereby pulling the co-ions into the bound state, *n* increases with $[S]$ to ultimately yield *N* at very high concentrations. For most other mechanisms, the discriminatory power of the Hill analysis is weak (Online supplemental material file S5.6) but, nevertheless, should be consistent with the other data.

Determination of underlying constants

The dependence of the apparent kinetic parameters from the substrate- and co-ion–dependent rate measurements on the second substrate largely determines the kinetic scheme underlying the transport mechanism. Analysis of the relation between the apparent kinetic parameters and substrate or co-ion concentration results in a set of constants (Table 5) that consist of a combination of $K_D{}^{S}$, $K_D{}^{H}$, α, β, β_1, β_2, and γ that is a characteristic of a particular kinetic scheme. (Online supplemental material, Table S5.9, gives examples.) In general, the kinetic schemes are overparameterized, and only in rare cases do the experimental data allow assigning numbers to individual constants in the scheme. Mostly, by comparing different constants deduced from the data, ranges of possible values may be indicated or consistent combinations suggested, which is relevant, especially for the α and γ parameters when values significantly smaller or larger than 1 can be assigned (LeVine et al., 2016). Then, the data indicate structural interaction between different binding sites resulting in positive or negative cooperativity.

Online supplemental material

This manuscript is accompanied by an Appendix on data analysis, an executable McHill file, and five files with supplemental information: S1 and S2 contain information on how to determine the *q* parameters, S3 presents the relation between co-ion binding and the rate equation, S4 contains extended information on the Hill coefficient, and S5 gives examples of more elaborate kinetic schemes.

Acknowledgments

This work was supported by the Netherlands Organization for Scientific Research (grants 865.11.001 and 714.018.003) and the European Research Council (starting grant 282083) .

The authors declare no competing financial interests.

Author contributions: J.S. Lolkema and D.J. Slotboom contributed to all stages of the work.

José D. Faraldo-Gómez served as editor.

Submitted: 29 June 2018
Revised: 25 October 2018
Accepted: 11 December 2018

References

Abramson, J., I. Smirnova, V. Kasho, G. Verner, H.R. Kaback, and S. Iwata. 2003. Structure and mechanism of the lactose permease of Escherichia coli. *Science.* 301:610–615. https://doi.org/10.1126/science.1088196

Accardi, A., and C. Miller. 2004. Secondary active transport mediated by a prokaryotic homologue of ClC Cl- channels. *Nature.* 427:803–807. https://doi.org/10.1038/nature02314

Canul-Tec, J.C., R. Assal, E. Cirri, P. Legrand, S. Brier, J. Chamot-Rooke, and N. Reyes. 2017. Structure and allosteric inhibition of excitatory amino acid transporter 1. *Nature.* 544:446–451. https://doi.org/10.1038/nature22064

Cleland, W.W. 1963. The kinetics of enzyme-catalyzed reactions with two or more substrates or products. I. Nomenclature and rate equations. *Biochim. Biophys. Acta.* 67:104–137. https://doi.org/10.1016/0926-6569(63)90211-6

Drew, D., and O. Boudker. 2016. Shared molecular mechanisms of membrane transporters. *Annu. Rev. Biochem.* 85:543–572. https://doi.org/10.1146/annurev-biochem-060815-014520

Fitzgerald, G.A., C. Mulligan, and J.A. Mindell. 2017. A general method for determining secondary active transporter substrate stoichiometry. *eLife.* 6:e21016. https://doi.org/10.7554/eLife.21016

Forrest, L.R., R. Krämer, and C. Ziegler. 2011. The structural basis of secondary active transport mechanisms. *Biochim. Biophys. Acta.* 1807:167–188. https://doi.org/10.1016/j.bbabio.2010.10.014

Garaeva, A.A., G.T. Oostergetel, C. Gati, A. Guskov, C. Paulino, and D.J. Slotboom. 2018. Cryo-EM structure of the human neutral amino acid transporter ASCT2. *Nat. Struct. Mol. Biol.* 25:515–521. https://doi.org/10.1038/s41594-018-0076-y

Groeneveld, M., and D.J. Slotboom. 2010. Na(+):aspartate coupling stoichiometry in the glutamate transporter homologue Glt(Ph). *Biochemistry.* 49:3511–3513. https://doi.org/10.1021/bi100430s

Hill, A.V. 1910. The possible effects of the aggregation of the molecules of hemoglobin on its dissociation curves. *J. Physiol.* 40:i–iv.

Krishnamurthy, H., and E. Gouaux. 2012. X-ray structures of LeuT in substrate-free outward-open and apo inward-open states. *Nature.* 481:469–474. https://doi.org/10.1038/nature10737

Kumar, H., V. Kasho, I. Smirnova, J.S. Finer-Moore, H.R. Kaback, and R.M. Stroud. 2014. Structure of sugar-bound LacY. *Proc. Natl. Acad. Sci. USA.* 111:1784–1788. https://doi.org/10.1073/pnas.1324141111

Kuriyan, J., B. Konforti, and D. Wemmer. 2013. The Molecules of Life. Garland Science, New York and London.

LeVine, M.V., M.A. Cuendet, G. Khelashvili, and H. Weinstein. 2016. Allosteric mechanisms of molecular machines at the membrane: Transport by sodium-coupled symporters. *Chem. Rev.* 116:6552–6587. https://doi.org/10.1021/acs.chemrev.5b00627

Lolkema, J.S., and D.J. Slotboom. 2015. The Hill analysis and co-ion-driven transporter kinetics. *J. Gen. Physiol.* 145:565–574. https://doi.org/10.1085/jgp.201411332

Malinauskaite, L., S. Said, C. Sahin, J. Grouleff, A. Shahsavar, H. Bjerregaard, P. Noer, K. Severinsen, T. Boesen, B. Schiøtt, et al. 2016. A conserved leucine occupies the empty substrate site of LeuT in the Na(+)-free return state. *Nat. Commun.* 7:11673. https://doi.org/10.1038/ncomms11673

Middendorf, T.R., and R.W. Aldrich. 2017a. Structural identifiability of equilibrium ligand-binding parameters. *J. Gen. Physiol.* 149:105–119. https://doi.org/10.1085/jgp.201611702

Middendorf, T.R., and R.W. Aldrich. 2017b. The structure of binding curves and practical identifiability of equilibrium ligand-binding parameters. *J. Gen. Physiol.* 149:121–147. https://doi.org/10.1085/jgp.201611703

Perez, C., C. Koshy, O. Yildiz, and C. Ziegler. 2012. Alternating-access mechanism in conformationally asymmetric trimers of the betaine transporter BetP. *Nature.* 490:126–130. https://doi.org/10.1038/nature11403

Ressl, S., A.C. Terwisscha van Scheltinga, C. Vonrhein, V. Ott, and C. Ziegler. 2009. Molecular basis of transport and regulation in the Na(+)/betaine symporter BetP. *Nature.* 458:47–52. https://doi.org/10.1038/nature07819

Reyes, N., C. Ginter, and O. Boudker. 2009. Transport mechanism of a bacterial homologue of glutamate transporters. *Nature.* 462:880–885. https://doi.org/10.1038/nature08616

Segel, I.H. 2014. Enzyme Kinetics. John Wiley and Sons, New York.

Verdon, G., and O. Boudker. 2012. Crystal structure of an asymmetric trimer of a bacterial glutamate transporter homolog. *Nat. Struct. Mol. Biol.* 19:355–357. https://doi.org/10.1038/nsmb.2233

Weiss, J.N. 1997. The Hill equation revisited: Uses and misuses. *FASEB J.* 11:835–841. https://doi.org/10.1096/fasebj.11.11.9285481

Wöhlert, D., M.J. Grötzinger, W. Kühlbrandt, and Ö. Yildiz. 2015. Mechanism of Na(+)-dependent citrate transport from the structure of an asymmetrical CitS dimer. *eLife.* 4:e09375. https://doi.org/10.7554/eLife.09375

Wyman, J., and S.J. Gill. 1990. Binding and Linkage: Functional Chemistry of Biological Macromolecules. University Science Books, Mill Valley, CA.

Yernool, D., O. Boudker, Y. Jin, and E. Gouaux. 2004. Structure of a glutamate transporter homologue from Pyrococcus horikoshii. *Nature.* 431:811–818. https://doi.org/10.1038/nature03018

Yifrach, O. 2004. Hill coefficient for estimating the magnitude of cooperativity in gating transitions of voltage-dependent ion channels. *Biophys. J.* 87:822–830. https://doi.org/10.1529/biophysj.104.040410

Zhang, Z., Z. Tao, A. Gameiro, S. Barcelona, S. Braams, T. Rauen, and C. Grewer. 2007. Transport direction determines the kinetics of substrate transport by the glutamate transporter EAAC1. *Proc. Natl. Acad. Sci. USA.* 104:18025–18030. https://doi.org/10.1073/pnas.0704570104